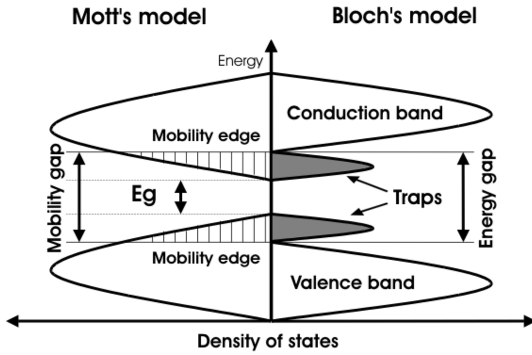

Fig. 3. Qualitative comparison between the Mott's model and the proposed one.

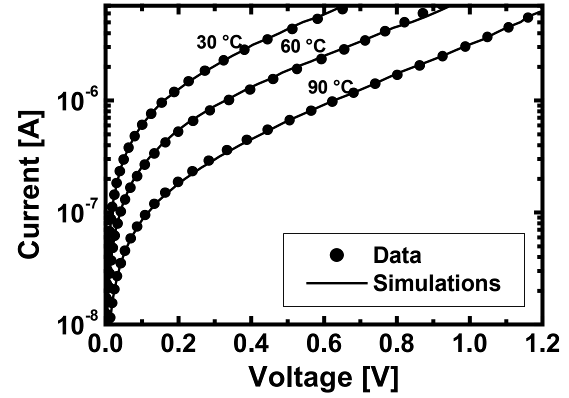

Fig. 4. Agreement of simulated and measured low field amorphous electrical characteristics for different temperatures (T=30, 60, 90 °C).

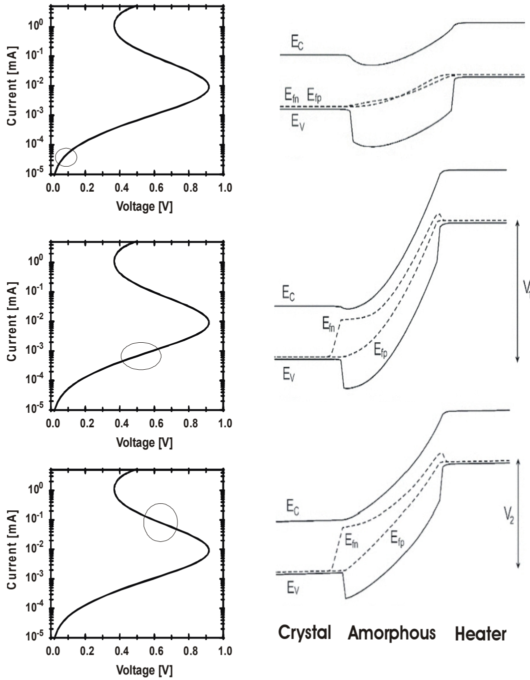

Fig. 5. Physical view of electronic switching. After the switching event, generation is sustained by free carriers with a reduced field.

II. ELECTRICAL MODEL

Due to its long range atomic order, the electron dynamics in the c-GST can be treated according to the Bloch's theorem as in a crystalline semiconductor[1]. On the other hand, a-GST does not show long range periodicity. However, investigations on amorphous compounds demonstrated the existence of localized states with variable transport properties [2]. It became thus a common practice in the '60 to describe these materials as in Fig.3-left [2], where "mobility edges" separate fully conductive bands from low mobility states. However, by assuming that low mobility localized states behave like trapping centers and that more conductive levels resemble delocalized states, a band structure can be employed to model the a-GST as a "very defective" crystalline semiconductor [1] (Fig.3-right). Moreover, amorphous GST presents other peculiar electrical transport properties, as shown by the low-field I-V curve of the OFF-state reported in Fig.4. Till about 200 mV, a linear behavior is found, while for higher voltages the current increases exponentially up to threshold switching. The exponential relationship between current and applied voltage is probably due to a carrier generation mechanism such as impact ionization, Poole-Frenkel or tunneling from contacts. To explain both the low-field behavior and the threshold switching effect, a field-assisted generation mechanism sustained by the free carrier concentration (e.g., avalanche ionization) must be invoked [5]. The competitive interaction between this generation mechanism and a strong Shockley-Hall-Read (SHR) recombination caused by the large defect density is responsible for the SNDC behavior in Fig.2. Based on the similarities between the properties of the a-GST and standard semiconductors, we have thus achieved a description of the a-GST fully compatible with models already employed for crystals, suitable to be implemented in a standard device simulator [3]. The accurate tailoring on experimental data of the material parameters, such as energy gap, carrier mobilities and density of states has been extensively discussed in our previous work [1]. The calibrated semiconductor-like model is able to provide a good agreement with measurements, as shown, for instance, in Fig. 4. Moreover, the SNDC curve reported in Fig.2 can be explained through a physical insight into the dynamics of the electronic switching mechanism (Fig.5). For low applied fields, a-GST quasi Fermi levels are close to their equilibrium position (Fig.5-top), resulting into an ohmic behavior. With this bias the generation and recombination rates are low and can be safely neglected. Increasing the voltage, the generation significantly increases due to the applied field, thus requiring to be balanced by a much higher recombination. The quasi Fermi levels thus split and move close to the de-localized bands (Fig.5 middle). Since the recombination mechanism depends on the unfilled defects density, at high applied field recombination is strongly reduced (all defects filled), and it can only partially balance the generation rate. The system thus reacts reducing the voltage drop to maintain the balance between recombination and generation, leading to the electronic switching. Generation is now sustained by a large density of free

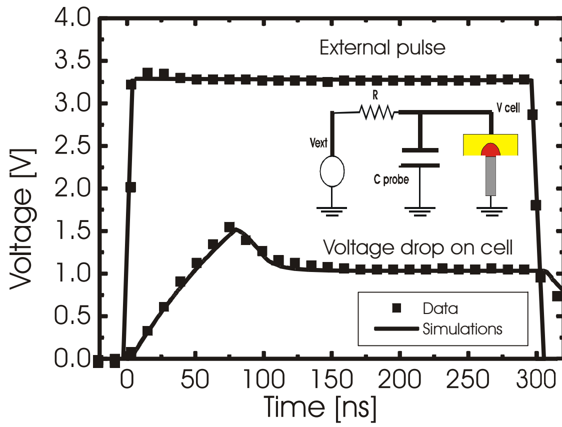

Fig. 6. Experimental and simulated programming transient pulse. The probe capacitance (about 25 pF) causes a delay in the switching event.

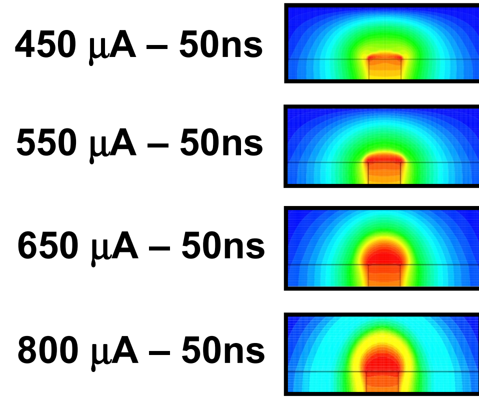

Fig. 7. Thermal maps obtained at the end of a 50ns pulse for increasing current pulses, with transient simulations. Red color corresponds to melting temperature (680 °C).

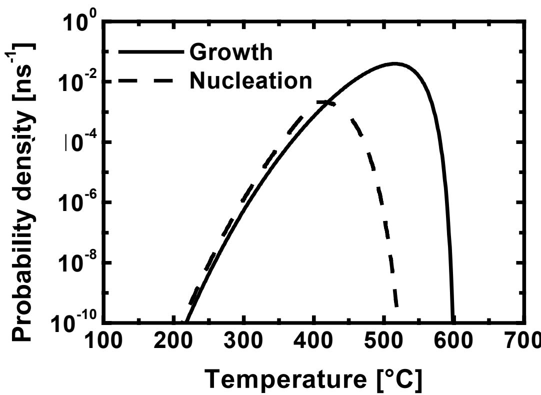

Fig. 8. Probability densities for unit of time for nucleation and growth.

carriers, with the electron quasi Fermi level close to the conduction band edge (Fig.5 bottom). Fig.6 shows that the numerical model correctly describes the pulsed operation mode of PCM cells. The agreement was achieved by a mixed-mode simulation, driving the PCM-cell with a load resistor of 4 kΩ. A capacitor of 25 pF was added to the Spice net between the cell top electrode and ground, describing the role of the probe tip capacitance, as depicted in the inset of Fig. 6. The capacitance causes a delay in the switching event of about 70 ns. The voltage drop on GST during the pulse plateau is instead determined by the partition between the load resistance and the ON-state amorphous resistance of about
1 kΩ.

III. Thermal and Phase Transition Model

To achieve a full description of the PCM programming functionality, the heat conduction equation has been self-consistently coupled with the electrical model to describe self-heating (Joule effect). Thermal maps can thus be obtained performing transient simulations on an initially crystalline device for several current values, as reported in Fig.7. In the first frame the melting condition may be recognized, corresponding to the existence of a thin melted layer of GST close to the interface with the metallic pillar. The transition from the melted phase to the amorphous one is determined by the quenching time. In fact, during the falling edge, the GST cools down passing through the crystallization temperature region, thus allowing nucleation and growth to take place with their own kinetics. If the falling edge is very short (10-15 ns), crystallization is practically avoided, so that the hot region becomes a-GST, resulting in a low conductive state. Further increase in the programming current causes the thermal spot to extend and the amorphous zone is correspondingly enlarged, still maintaining a hemispherical shape. To account for the phase transitions responsible for the memory effect, a local phase-change algorithm has been coupled to the electro-thermal equations. The crystallization takes place by the action of nucleation and growth. The first phenomenon refers to the appearance of nuclei of the new phase in a homogeneous matrix of the old phase, while the second one refers to the growth of a pre-existing interface between the new and the old phases. In the low temperature range, due to the increase of the atomic mobility with temperature inside the melted GST, both nucleation and growth are enhanced with temperature (Fig. 8). At each temperature, a critical dimension exists for which a cluster of coordinated material is stable and thus becomes a nucleus. The stability of a cluster comes from the balance between the negative free volume energy contribution related to the phase transition (crystal is the stable phase), and the positive work to build the surface of crystal cluster. This critical dimension increases with temperature, and, close to the melting condition, practically no stable nuclei may exist (Fig.8), resulting in a growth driven crystallization. Starting from the model originally proposed in [4], a Montecarlo algorithm for both nucleation and growth has been implemented and calibrated on experimental data. The grid elements dimension was chosen to be comparable with the critical cluster size at the temperature for which nucleation probability shows its maximum. The probability densities for unit of time are reported in Fig.8.

IV. Results

To couple the phase change transition and the electro-thermal model, an external loop was implemented as